ASEAN Journal of Science and Engineering

Journal homepage: http://ejournal.upi.edu/index.php/AJSE/

Effect of Sintering Conditions on the Structural and Morphological Characteristics of Hydroxyapatite Synthesized from Belida Fish (*Chitala lopis*) Bone

Ratna Kusumawardani[1,2], Atiek Rostika Noviyanti[1,3,], Mukhamad Nurhadi[2], Akrajas Ali Umar[4],Ferli Septi Irwansyah[5], Muhamad Diki Permana[6]*

[1]Universitas Padjajaran, Sumedang, Indonesia
[2]Universitas Mulawarman, Samarinda, Indonesia
[3]Badan Riset dan Inovasi Nasional, Indonesia
[4]Universiti Kebangsaan Malaysia, Bangi, Malaysia
[5]UIN Sunan Gunung Djati, Bandung, Indonesia
[6]University of Yamanashi, Kofu, Japan
Correspondence: E-mail: atiek.noviyanti@unpad.ac.id

ABSTRACT

Hydroxyapatite (HA) was synthesized from *Chitala lopis* (belida fish) bone waste as a sustainable and low-cost natural source, and the effects of sintering temperature and atmosphere on its properties were evaluated. Bone powder was sintered at 600–1000°C under open crucible (FBO) and closed crucible (FBC) conditions. X-ray diffraction (XRD) and Fourier-transform infrared spectroscopy (FTIR) confirmed HA formation, with crystallinity and crystal size increasing at higher temperatures. Scanning electron microscopy (SEM) revealed morphological evolution from porous, irregular structures at lower temperatures to denser, more compact morphologies at higher temperatures. FBO conditions promoted larger crystallites and oriented growth, whereas FBC enhanced densification and reduced porosity. X-ray fluorescence (XRF) detected trace elements (Zn, Fe, Ti) potentially beneficial for bioactivity. Findings indicate that both sintering temperature and atmosphere significantly influence HA purity, crystallinity, and morphology, enabling property optimization for applications from porous adsorbents to dense bone implant materials.

ARTICLE INFO

Article History:
Submitted/Received 05 May 2025
First Revised 02 Jun 2025
Accepted 04 Aug 2025
First Available online 05 Aug 2025
Publication Date 01 Dec 2025

Keyword:
Crystallinity,
Fish bone,
Grain size,
Hydroxyapatite,
Sintering.

1. INTRODUCTION

Hydroxyapatite (HA), with the chemical formula $Ca_{10}(PO_4)_6(OH)_2$, is a naturally occurring mineral of the apatite family and is predominantly found in hard tissues such as bone and teeth [1]. Among the various biomaterials in the apatite group, HA has emerged as a highly promising candidate, particularly in bone tissue engineering [2] and dental applications [3]. It is typically white to off-white and possesses a molecular weight of 502.31 g/mol, a Mohs hardness of 5, and a density of approximately 3.16 g/cm^3 [4]. The material's calcium-to-phosphorus (Ca/P) ratio of 1.67 is considered ideal for promoting new bone growth, making HA suitable for biomedical applications such as bone grafts and implants, especially in cases involving trauma, tumors, or congenital disorders [5, 6]. HA is thermodynamically stable in its crystalline form under physiological conditions and exhibits a composition closely resembling that of natural bone mineral [7]. Owing to these characteristics, HA has garnered significant attention in recent years, not only for biomedical purposes but also for applications in the environmental and catalytic fields. In catalysis, HA has been employed in various chemical reactions, including condensation, oxidation, and photocatalysis [8, 9]. Furthermore, in environmental remediation, apatite-based materials have demonstrated effectiveness in removing heavy metals, organic pollutants, and dyes from contaminated water and soil [10]. Recent developments have expanded the use of HA in broader environmental applications, targeting the purification of air [11], soil [12, 13], and water [14, 15].

HA can be obtained from both natural and synthetic sources. In recent years, there has been growing interest in the development of HA from natural materials due to their compositional similarity to human bone. Naturally derived HA is typically non-stoichiometric and contains trace elements such as Na^+, Zn^{2+}, Mg^{2+}, K^+, Si^{4+}, Ba^{2+}, F^-, and CO_3^{2-}, which can enhance its bioactivity and functionality in biomedical applications [16, 17]. Moreover, natural HA exhibits high ion-exchange capacity and adsorption ability [17, 18], making it suitable for various environmental and biomedical uses. Additionally, it is considered more environmentally friendly [19], safer for biomedical applications, and more cost-effective compared to synthetic alternatives [20, 21]. Natural sources of HA include waste derived from animals such as cow bones [22], pig bones [23], camel bones [24], goat bones [25], sheep bones [26], and fish bones [27], including their scales [28]. Other biological wastes, such as eggshells [1], shellfish [29], crab shells [30], and snail shells [31], have also been explored as alternative precursors for HA synthesis. The utilization of these bio-wastes not only provides a sustainable route for HA production but also supports waste valorization and circular economy practices. On the other hand, HA can also be synthesized from synthetic precursors using chemical sources of calcium and phosphate [32, 33]. Although synthetic HA offers the advantage of controlled morphology and purity tailored to specific applications [34-36], it is generally more costly. To improve the environmental sustainability of synthetic HA production, researchers have employed green templating agents derived from plant sources, including roots, stems, and leaves [37].

Based on previous studies [38-41], this study focused on the synthesis of HA from fish bones, which are an abundant and readily available biowaste. The use of fish bone as a raw material offers advantages in terms of sustainability and cost-effectiveness, aligning with efforts to utilize waste-derived resources in environmentally friendly applications [20, 42, 43]. Extraction of HA from fish bones in this research is carried out using the sintering method. Sintering plays a crucial role in processing fish bone–derived HA, as it transforms raw bone powder into a denser, more mechanically stable bioceramic suitable for biomedical and environmental applications [44]. The primary advantage of sintering lies in the consolidation

DOI: https://doi.org/10.17509/ajse.v5i3.88775
p- ISSN 2776-6098 e- ISSN 2776-5938

of HA particles through thermal treatment, which enhances mechanical strength, reduces porosity, and improves the material's handling properties compared to its unsintered counterpart [45]. This densification is achieved via atomic diffusion at elevated temperatures, facilitating particle bonding and the formation of a robust crystalline structure.

Several factors significantly influence the sintering process and, consequently, the final structural and morphological characteristics of HA. Among these, temperature is one of the most critical parameters, as it directly affects the yield and crystallinity of the resulting HA. Higher sintering temperatures generally promote particle compaction and grain growth, leading to an increase in crystallinity, improved hardness, and reduced porosity [46]. However, excessively high temperatures can cause the decomposition of HA into secondary calcium phosphate phases such as tricalcium phosphate (TCP), which may adversely affect its bioactivity [47]. In addition to temperature, sintering time also plays a vital role. Sufficient duration is necessary to allow for atomic diffusion, facilitating densification and phase purity. However, prolonged sintering can result in undesirable grain coarsening and phase transformations [48]. Another important factor is the sintering atmosphere, which can be manipulated through open-cup (ambient air) or closed-cup (sealed) conditions. Open-cup sintering is more commonly used, but it can cause the loss of volatile components or oxidation at high temperatures. Conversely, closed-cup sintering can maintain a more controlled atmosphere, thereby potentially minimising HA decomposition and influencing the final phase composition and microstructure. Several studies have emphasised the importance of optimising sintering parameters to tailor HA properties for specific applications, particularly in bone. The novelty of this study lies in its comparative approach to evaluating the influence of open-cup and closed-cup sintering atmospheres on the physicochemical characteristics and morphology of HA derived from *Chitala lopis* bone, by systematically examining.

2. METHODS

2.1. Materials

The chemicals used for the preparation of HA include belida fish (*Chitala lopis*) bones obtained from Amplang manufacturing waste in Samarinda, Indonesia; distilled water; and technical-grade acetone (C_3H_6O) in 1 L packaging.

2.2. Synthesis of Hydroxyapatite (HA)

Fish bone waste is separated from other waste, washed, and cleaned by boiling it in water for 1 hour to facilitate the removal of organic substances and fats adhering to its surface [49, 50]. The clean bones are dried in an oven at 60°C for 48 hours. The dried bones are soaked in acetone for 3 × 24 hours, with the solvent replaced every 24 hours, to reduce any remaining organic matter still adhering to them. **Figure 1a** and **Figure 1b** show the difference between dried fish bones before and after washing with acetone. The clean bones were then washed with distilled water until the wash water reached neutral pH. The bones were dried, ground using a blender, and sieved through a 100-mesh sieve [51]. The resulting powder is considered crude HA (FB). To increase the HA content, a purification step is performed by sintering FB in a furnace at 600–1000°C for 4 hours, with a heating rate of 5°C/minute [52]. The samples before and after sintering exhibited colour differences, as shown in **Figure 1c**. FB was sintered under different temperature conditions (600–1000°C) and sintered with an open crucible (FBO) and a closed crucible (FBC). The samples were then coded as shown in **Table 1**. Based on **Table 1**, it is evident that the sintering method caused a decrease in sample mass due to the evaporation of organic matter.

DOI: https://doi.org/10.17509/ajse.v5i3.88775
p- ISSN 2775-6793 e- ISSN 2775-6815

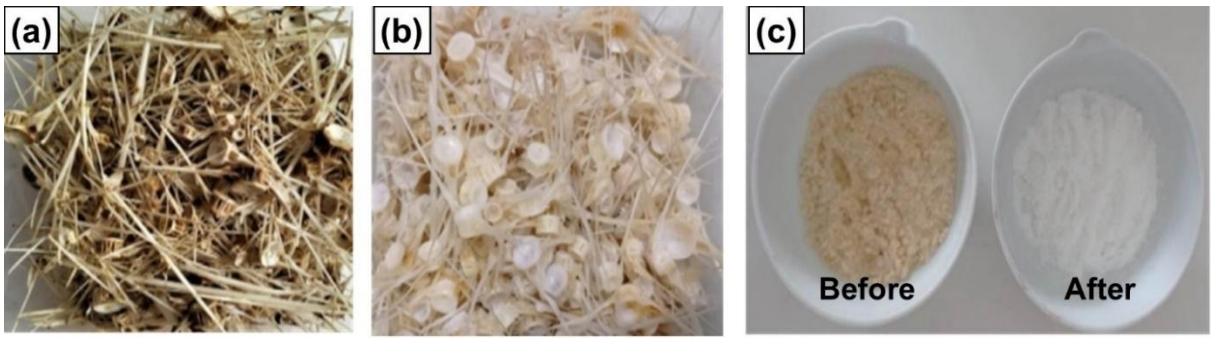

Figure 1. (a) Coarse fish bone, (b) fish bone after soaking in acetone, and (c) color difference of fish bone powder before sintering and after sintering.

Table 1. HA code of sintering results.

Sample Code	Mass before sintering (g)	Sintering condition	Sintering temperature (°C)	Sintering time (h)	Mass after sintering (g)	Yield (%)	Color after sintering
FB	-	-	-	-	-	-	Pale yellow
FBO-600	20.0084	Open	600	4	11.4067	57.01	Light brown
FBO-700	20.0155	Open	700	4	10.9787	54.85	Grayish white
FBO-800	20.0016	Open	800	4	10.9707	54.85	Grayish white
FBO-900	20.0026	Open	900	4	10.9382	54.68	White
FBO-1000	20.0039	Open	1000	4	10.9058	54.52	White
FBC-600	20.0079	Closed	600	4	11.3661	56.81	Grayish brown
FBC-700	20.0046	Closed	700	4	11.3684	56.83	Black with a little white
FBC-800	20.0009	Closed	800	4	11.1619	55.81	White
FBC-900	20.0003	Closed	900	4	11.0061	55.03	White
FBC-1000	20.0020	Closed	1000	4	10.9482	54.74	White

2.3. Characterizations

Thermogravimetric analysis (TGA) curves of the samples were obtained on a Thermo plus (TG-DTA8120, Rigaku) with a heating rate of 10°C/min. To determine the functional groups of the sample, characterization was carried out using Fourier-transform infrared spectroscopy (FTIR). The FTIR analysis was conducted using an IRPrestige-21, Shimadzu. The results are presented as transmittance spectra over a wavelength range of 400–4000 cm^{-1}. The samples were characterized using powder X-ray diffraction (XRD, X'Pert Pro, PanAnalytical). Data were collected from 2θ = 8° to 65° at room temperature. To confirm the crystal structure, the Debye–Scherrer method was applied by analyzing the diffraction patterns at specific 2θ° and their corresponding intensities. The crystallite size (D) was calculated using the Scherrer equation, as shown in Equation 1, where K is the Scherrer constant (typically 0.9), λ is the X-ray wavelength (1.5406 Å for Cu Kα radiation), B is the full width at half maximum (FWHM) of the diffraction peak in radians, and θ is the Bragg angle. Furthermore, the degree of crystallinity can be estimated using Equation 2, where Ac is the area under the crystalline peaks and At is the total area (crystalline + amorphous) of the diffraction pattern. Analysis of the diffraction peaks obtained for HA was performed by comparing the results with standard reference data from the ICSD database for phase identification [53]. The elemental composition of the samples was analyzed using X-ray fluorescence spectrometry (XRF). The morphology of the samples was measured using a scanning electron microscope (SEM, TM3030 Plus, Hitachi, Tokyo, Japan).

DOI: https://doi.org/10.17509/ajse.v5i3.88775
p- ISSN 2776-6098 e- ISSN 2776-5938

$$D = \frac{K\lambda}{B\ cos\theta} \quad (1)$$

$$Xc = \frac{Ac}{At} \times 100\% \quad (2)$$

3. RESULTS AND DISCUSSION

3.1. Visual Observation and Thermal Behavior

The sintering process of fish bone powder is carried out at various temperatures (600–1000°C) for 4 hours to convert organic material into crystalline hydroxyapatite (HA). The visual changes shown in **Figure 2** indicate that the temperature and conditions of the crucible during the sintering process greatly affect the HA produced. At lower temperatures (600–700°C), the samples appear dark or black, indicating the presence of residual organic material. As the sintering temperature increased above 700°C, a significant change in color was observed—the samples became progressively whiter, signifying more complete removal of organic components and the formation of purer HA. The whitest appearance was observed at the highest sintering temperatures (800–1000°C), suggesting that higher temperatures facilitate a greater degree of HA crystallization and purity. This observation aligns with prior reports [54-56], where high organic content (>30%) in fish bones contributes to coloration and odor, both eliminated upon thermal treatment. The degradation of these organics during sintering results in a cleaner inorganic matrix and the progressive development of the HA phase.

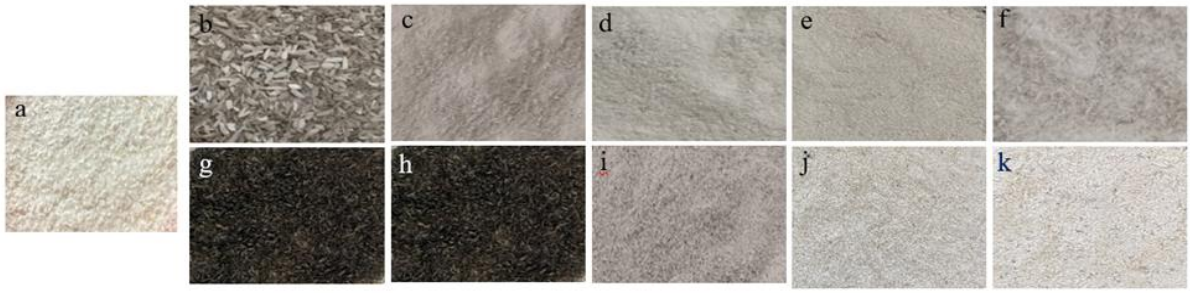

Figure 2. Color change of samples (a) FB, (b) FBO-600, (c) FBO-700, (d) FBO-800, (e) FBO-900, (f) FBO-1000, (g) FBC-600, (h) FBC-700, (i) FBC-800, (j) FBC-900, and (k) FBC-1000.

The experimental results showed that high-temperature treatment effectively removed most of the residual organic matter in the samples, as evidenced by changes in colour and odour, as well as a reduction in mass of approximately 45%. Thermogravimetric analysis (TGA) confirmed this transformation process. **Figure 3a** shows the TGA profile of raw fish bone, indicating three main stages of mass loss: (i) water evaporation between 25–200°C (~8%), (ii) decomposition of organic material (protein, lipids, and collagen) between 200–550°C (32.5%), and (iii) de-hydroxylation of HA between 550–800°C (~2%). This phenomenon aligns with the research conducted by previous study [25]. The remaining material after this stage primarily consists of inorganic components, hydroxyapatite, along with other thermally stable inorganic constituents. In conclusion, the TGA results indicate that fish bone powder contains absorbed water, a significant amount of organic compounds (estimated at approximately 32% of the initial mass), and thermally stable inorganic phases, hydroxyapatite. These results indicate that sintering above 700°C is crucial for effectively removing organic material and enhancing the purity of HA from *Chitala lopis* fish bones. FTIR spectra of the raw fish bone powder (FB) in **Figure 3b** showed the presence of both organic and inorganic functional groups. The broad absorption at 3000–3800 cm^{-1} corresponds to O–H stretching vibrations, while the bands at 2924 and 2853 cm^{-1} are attributed to aliphatic –CH_2 stretching. Carbonyl groups (C=O) were

DOI: https://doi.org/10.17509/ajse.v5i3.88775
p- ISSN 2775-6793 e- ISSN 2775-6815

detected at 1650 and 1460 cm^{-1}, and phosphate (PO_4^{3-}) vibrations were observed at around 1090 cm^{-1}. These findings confirm that the raw fish bone comprises both organic matter and HA components [57].

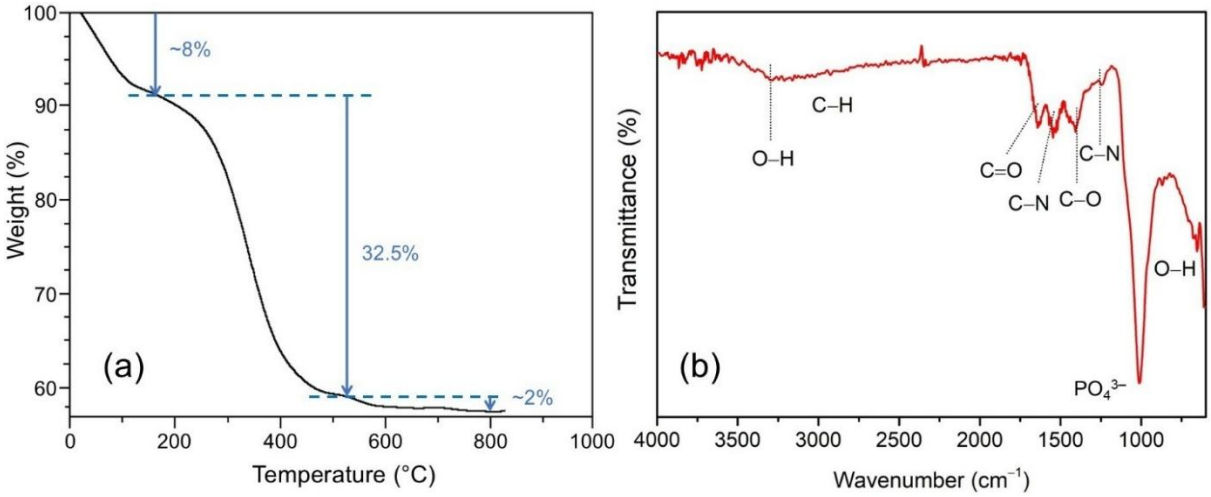

Figure 3. (a) TGA and (b) FTIR spectra of fish bone before calcination (FB).

3.2. Functional Group Analysis

The FTIR spectrum of sintered FB is shown in **Figure 4**. Based on **Figure 4**, the asymmetric stretching lines of phosphate (PO_4^{3-}) at 1030–1090 cm^{-1}, symmetric stretching around 960 cm^{-1}, and bending vibrations at 560–600 cm^{-1} are clearly identified in all samples [58]. A small absorption peak around 1450 cm^{-1} indicates the presence of carbonate groups in the samples before and after burning. Additionally, a minor OH– OH-vibration peak was observed near 630 cm^{-1} [34]. This FTIR spectrum confirms the formation of HA under both open (FBO) and closed (FBC) sintering conditions, as indicated by the presence of characteristic absorption bands corresponding to hydroxyl (OH–), phosphate (PO_4^{3-}), and carbonate (CO_3^{2-}) functional groups. The intensity and sharpness of the OH– and PO_4^{3-} peaks increase with higher sintering temperatures, particularly in the FBO sample, indicating enhanced crystallinity and phase purity under open conditions. The carbonate band in the 1420–1460 cm^{-1} range is more prominent in closed-sintered (FBC) samples, indicating that limited gas exchange in a closed environment can lead to CO_2 accumulation, thereby promoting the replacement of some phosphate or hydroxyl groups by carbonate ions in the HA lattice. Conversely, open sintering (FBO) allows for better air circulation around the sample, facilitating the release of CO_2 generated from the decomposition of carbonates and organic matter. This continuous gas exchange promotes more complete decomposition of carbon-containing species. Additionally, residual carbon in samples sintered in open crucibles is more likely to oxidise into CO_2 in the presence of atmospheric oxygen and then be released, minimising carbonate formation and enhancing HA purity.

DOI: https://doi.org/10.17509/ajse.v5i3.88775
p- ISSN 2776-6098 e- ISSN 2776-5938

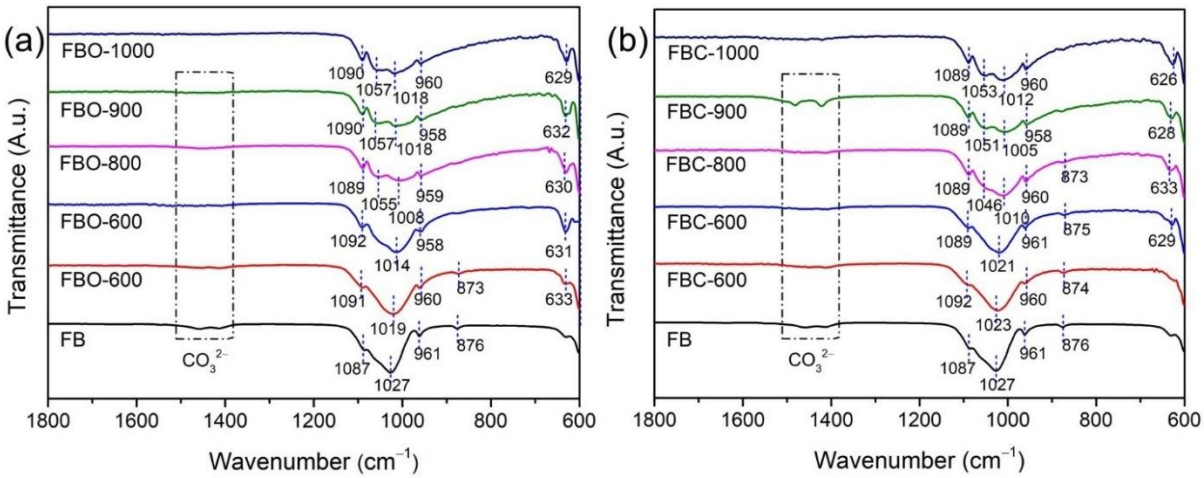

Figure 4. FTIR spectra of (a) FBO and (b) FBC with varying sintering temperatures.

3.3. Structural Identification

The XRD patterns of fish bone before and after sintering are shown in **Figure 5**. The sintered samples were indexed to the hexagonal hydroxyapatite (HA) phase (JCPDS No. 09-0432), with prominent diffraction peaks observed at 2θ = 25.8° (002), 31.7° (211), 32.1° (112), and 32.8° (300), among others. All samples exhibited a hexagonal crystal structure with a P63/m space group. The calcined samples showed the presence of both HA and β-tricalcium phosphate (β-TCP) phases under both sintering conditions [58]. The unsintered fish bone (FB) exhibited an amorphous pattern, which progressively transitioned to sharper and more intense peaks with increasing calcination temperature, indicating improved crystallinity. At lower sintering temperatures (600°C and 700°C), broader peaks were observed, whereas higher temperatures (900°C and 1000°C) produced sharper and more distinct peaks. As shown in **Figure 5a** and **Figure 5b**, FBO-600 still exhibited an amorphous pattern, while FBO-700 began to show sharp peaks, indicating enhanced crystallinity. Further increases in temperature (from 700°C to 1000°C) did not result in significant changes in the XRD patterns for the FBO samples, suggesting that crystallinity was largely achieved by 700°C.

Similarly, as seen in **Figure 5c** and **Figure 5d**, the FBC samples followed a trend comparable to that of the FBO series. However, under closed sintering conditions, FBC-700 still displayed relatively amorphous peaks, with high crystallinity only becoming evident at 800°C (FBC-800). Open-cup sintering appeared to promote the formation of more crystalline HA, while the closed-cup condition exhibited a delayed phase transformation, especially at lower temperatures. Crystallinity significantly influences the mechanical properties of ceramics for biomedical applications. Higher crystallinity is favorable for load-bearing implants, while lower crystallinity supports bone regeneration and enhanced biodegradability [59].

DOI: https://doi.org/10.17509/ajse.v5i3.88775
p- ISSN 2775-6793 e- ISSN 2775-6815

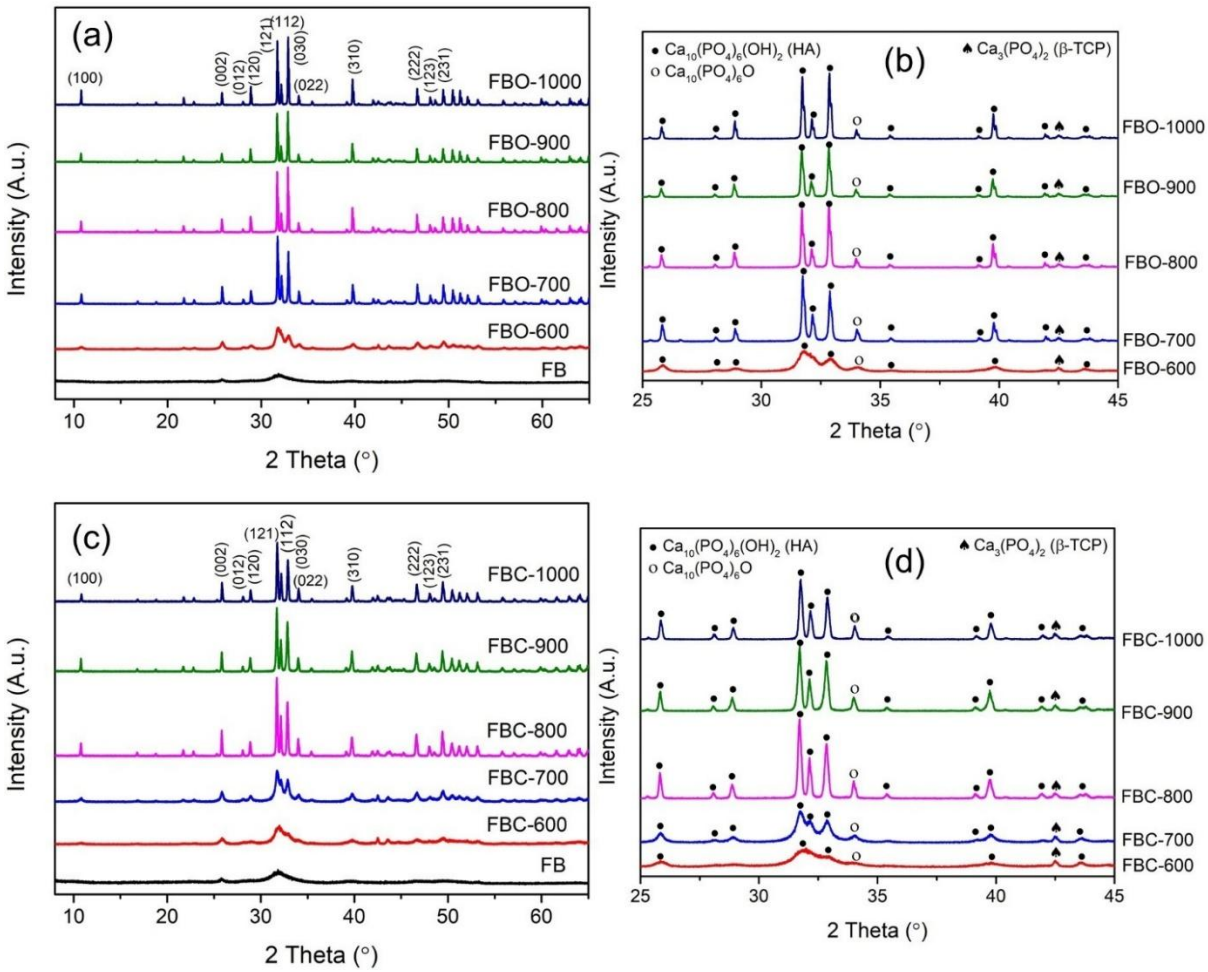

Figure 5. XRD pattern of (a,b) FBO and (c,d) FBC samples at varying sintering temperatures.

In addition to the HA phase, small amounts of tetracalcium phosphate (TTCP, $Ca_{10}(PO_4)_6O$) and β-tricalcium phosphate (β-TCP, $Ca_3(PO_4)_2$) were observed in the XRD patterns of samples at various sintering temperatures. These phases typically emerge at elevated sintering temperatures due to the dehydration and thermal decomposition of HA. Moreover, an imbalance in the Ca/P ratio can also contribute to the formation of TTCP and β-TCP [60, 61]. The decomposition of HA into TCP is represented by Equation 3.

$$Ca_{10}(PO_4)_6(OH)_2 \rightarrow 3Ca_3(PO_4)_2 + CaO + H_2O \quad (3)$$

The variation in crystallite size and crystallinity percentage of the samples at different calcination temperatures is shown in **Figure 6**. The crystallite size was estimated using the Scherrer equation based on the full width at half maximum (FWHM) of the main diffraction peak (Equation 1). The crystallite size increased with rising calcination temperature, reaching a maximum at 900°C for FBO samples and at 800°C for FBC samples, before slightly decreasing. For the FBO samples, crystallite sizes ranged from 23.9 to 75.2 nm, while for the FBC samples, they ranged from 19.3 to 69.4 nm. The crystallite size of FBO samples tended to be larger than that of FBC samples at the same temperature, indicating enhanced crystal growth under open sintering conditions. Furthermore, the increasing crystallinity with temperature was consistent with the FTIR and XRD observations.

DOI: https://doi.org/10.17509/ajse.v5i3.88775
p- ISSN 2776-6098 e- ISSN 2776-5938

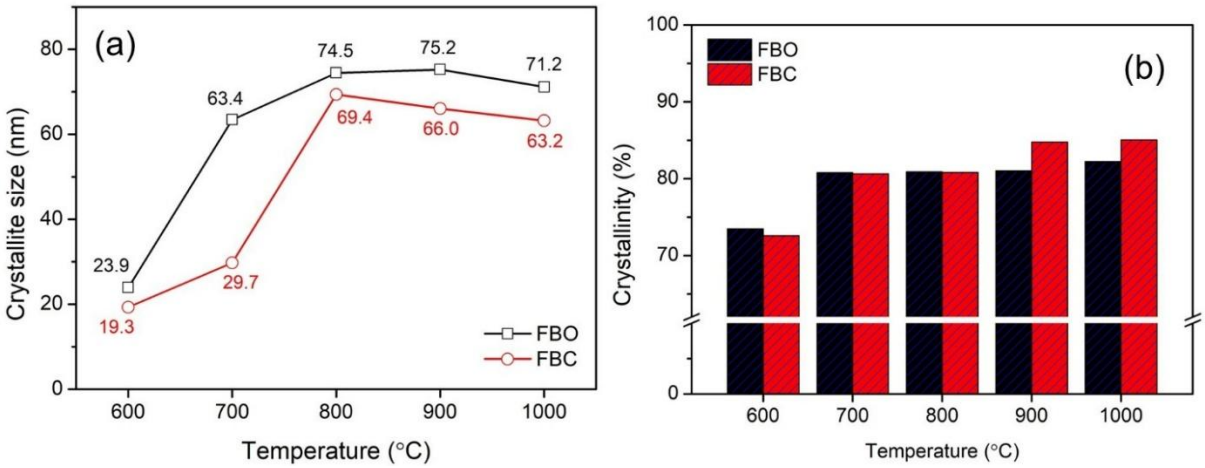

Figure 6. (a) Crystallite size and (b) crystallinity of FBO and FBC samples with varying sintering temperatures.

Table 2 presents the crystal properties of all samples. HighScore Plus software (PANalytical version 3.0.5) was used in conjunction with the Inorganic Crystal Structure Database (ICSD) to perform Rietveld refinement, while a shifted polynomial function coefficient was applied to fit the background [62]. The lattice parameters of HA remained consistent across all calcination temperatures, confirming the formation of a stable HA phase. Nevertheless, slight differences in unit cell volume were observed due to variations in calcination conditions. FBO samples exhibited slightly larger unit cell volumes (~1 $Å^3$) than FBC samples at all calcination temperatures.

Subsequently, the lattice strain (ε) was evaluated using the Williamson–Hall method (Equation 4) based on the (002) plane of HA [63]. Dislocation density was calculated using Equation 5, where δ is the dislocation density (m^{-2}) and D is the crystallite size (m). The specific surface area (SSA) was then determined using the Sauter equation (Equation 6), defined as the crystal surface area (SA) per unit mass, where ρ is the crystal density (g/m^3) [64].

$$\varepsilon = \frac{B\cos\theta}{4} \quad (4)$$

$$\delta = \frac{1}{D^2} \quad (5)$$

$$SSA = \frac{6}{D.\rho} \quad (6)$$

As shown in **Table 2**, with increasing temperature and crystallite size, both FBO and FBC samples exhibited lower dislocation density and lattice strain at higher temperatures, indicating a reduction in lattice defect concentrations. These intrinsic values reflect the number of dislocations in the material; hence, lower values indicate better material quality. The strain of each sample may vary due to various crystal defects such as interstitials, vacancies, dislocations, and layer fractures, which contribute to different levels of strain in the crystal [64]. Moreover, SSA is a crucial material property in surface-related reactions such as adsorption and sensing [65]. In this study, HA samples sintered at lower temperatures exhibited the highest SSA values, which gradually decreased with increasing sintering temperature.

DOI: https://doi.org/10.17509/ajse.v5i3.88775
p- ISSN 2775-6793 e- ISSN 2775-6815

Table 2. Crystal properties of FBO and FBC.

Sample code	Lattice parameter			Crystal strain/ε (10^{-3})[a]	δ (10^{14}m^{-2})[a]	*SSA* (m^2/g)[b]
	$a = b$ (Å)	c (Å)	V (Å^3)			
FB	-	-	-	1.45	17.58	-
FBO-600	9.4258(15)	6.8900(12)	530.14	1.45	17.49	79.66
FBO-700	9.4252(7)	6.8838(6)	529.59	0.55	2.49	30.03
FBO-800	9.4293(2)	6.8835(2)	530.03	0.47	1.80	25.58
FBO-900	9.4279(2)	6.8827(2)	529.81	0.46	1.77	25.31
FBO-1000	9.4271(2)	6.8854(2)	529.93	0.49	1.97	26.77
FBC-600	9.4154(7)	6.8836(6)	528.48	1.80	26.83	98.97
FBC-700	9.4184(1)	6.8831(1)	528.77	1.17	11.30	64.24
FBC-800	9.4185(1)	6.8827(1)	528.73	0.50	2.08	27.55
FBC-900	9.4180(1)	6.8831(1)	528.73	0.52	2.29	28.93
FBC-1000	9.4185(1)	6.8843(1)	528.88	0.55	2.50	30.22

calculated using Williamson-Hall method from (002) peak of HA, bcalculated using Sauter's method from (002) peak of HA.

3.4. Elemental Analysis

The atomic weight percentages of elements present in the samples at various calcination temperatures were determined by X-ray fluorescence (XRF) analysis and are presented in **Table 3**. The results show that the samples not only consist of major components such as calcium (Ca) and phosphorus (P), but also contain trace elements, including aluminum (Al), potassium (K), iron (Fe), zinc (Zn), and titanium (Ti) in the synthesized HA.

Table 3 shows in Ca/P ratios for FBO samples calcined at 600°C to 1000°C were 3.26, 3.24, 3.20, 3.19, and 3.16, respectively. For the FBC samples, the Ca/P ratios from 600°C to 1000°C were 3.34, 3.26, 3.16, 3.14, and 3.13, respectively. The decreasing trend in the Ca/P ratio with increasing calcination temperature may be attributed to the loss of water and hydroxyl groups from the crystal structure at elevated temperatures. A similar trend has also been observed by previous research groups [58]. It is worth noting that the ideal Ca/P ratio of stoichiometric hydroxyapatite is 1.67. The significantly higher Ca/P ratios observed in this study may indicate the formation of additional calcium phosphate phases, such as tetracalcium phosphate (TTCP), as confirmed by the XRD results.

In addition, the presence of trace elements such as Fe, Zn, Ti, Al, and K may also influence the physicochemical and biological properties of the synthesized HA. For instance, Zn^{2+} is known to enhance osteogenic activity and can contribute to improved bioactivity and antibacterial performance of HA-based biomaterials [66]. Fe contamination, often derived from processing equipment or raw material impurities, may influence the color and redox properties of the material [67]. Titanium and aluminum, though present in minor amounts, can potentially affect thermal stability and grain boundary behavior during sintering [68]. Potassium (K^+), typically associated with biological systems, may influence ionic conductivity and also indicate partial substitution within the HA lattice [69]. While these elements appear in trace quantities, their presence may subtly modify the structural or functional properties of HA, and therefore, their effects warrant further investigation in biomedical or environmental applications.

DOI: https://doi.org/10.17509/ajse.v5i3.88775
p- ISSN 2776-6098 e- ISSN 2776-5938

Table 3. Elemental composition of FBO and FBC.

Element	Wt (%)									
	FBO-600	**FBO-700**	**FBO-800**	**FBO-900**	**FBO-1000**	**FBC-600**	**FBC-700**	**FBC-800**	**FBC-900**	**FBC-1000**
Ca	78.87	78.98	78.81	79.13	79.10	79.60	78.84	78.89	79.00	78.92
P	18.67	18.82	19.01	19.14	19.36	18.41	18.67	19.27	19.43	19.44
Al	1.56	0.91	1.43	1.21	1.15	1.32	1.18	1.30	1.32	1.41
K	0.53	0.50	0.38	0.30	0.21	0.56	0.51	0.47	0.19	0.18
Fe	0.21	0.64	0.20	0.08	0.06	0.02	0.02	0.02	0.03	0.02
Zn	0.10	0.08	0.10	0.09	0.06	0.06	0.06	0.04	0.01	0.01
Ti	0.02	0.03	0.03	0.02	0.01	0.01	0.01	0.01	0.01	0.01
Ca/P ratio	3.26	3.24	3.20	3.19	3.16	3.34	3.26	3.16	3.14	3.13

3.5. Morphological Identification

The surface morphology of HA synthesized from fish bone at various temperatures and sintering conditions was observed using SEM, as shown in **Figure 7**. Under open sintering conditions (FBO), increasing the temperature from 800°C to 1000°C resulted in significant morphological changes. The FBO-800 sample exhibited a relatively rough and porous surface with randomly distributed plate-like structures. The particles began to agglomerate but still retained their shapes, leaving numerous gaps and pores. At 900°C (FBO-900), the morphology appeared more ordered, dominated by overlapping plate-like structures, similar to the results reported by other study [70]. Particle agglomeration was more pronounced, although surface porosity remained visible. At 1000°C (FBO-1000), the surface became denser with stronger particle agglomeration, forming larger and more oriented structures. Some regions exhibited clearer and more regular crystal growth resembling rods, while others retained fewer plate-like structures. Overall, surface porosity was reduced compared to samples sintered at lower temperatures.

In contrast, samples sintered under closed crucible conditions (FBC) displayed a different morphological trend. At 800°C (FBC-800), the morphology was dominated by very fine, agglomerated particles forming small clusters. The surface appeared more granular and less porous than FBO-800. At 900°C (FBC-900), a mixture of agglomerated fine particles and a limited number of larger plate-like structures was observed. Although similar in structure to FBO-900, FBC-900 exhibited a higher density of fine particles and more intense agglomeration, resulting in reduced porosity. At 1000°C (FBC-1000), the surface morphology became relatively uniform, with strongly agglomerated particles forming a dense structure. Some areas began to exhibit plate-like features, although the overall structure indicated significant particle fusion and substantial porosity reduction.

A direct comparison between FBO and FBC samples at the same sintering temperatures highlights the influence of atmospheric conditions on particle morphology. At 800°C, FBO-800 displayed a rougher and more porous surface with visible remnants of the original bone structure (plates), indicating that calcination and initial crystallization were more dominant under open conditions, thus preserving porosity. In contrast, FBC-800 showed finer particles with tighter agglomeration, producing a more granular and less porous surface. This may be attributed to limited gas exchange under closed conditions, which promoted the formation of smaller particles and tighter agglomerates. At 900°C, both samples exhibited growth of plate-like structures; however, FBC-900 contained a higher density of agglomerated fine particles in combination with plate-like structures, while FBO-900 appeared more homogeneous in its plate morphology. At 1000°C, both conditions yielded significantly denser materials. FBO-1000 showed oriented rod-like crystal growth with strong agglomeration, whereas FBC-1000

DOI: https://doi.org/10.17509/ajse.v5i3.88775
p- ISSN 2775-6793 e- ISSN 2775-6815

appeared highly dense and uniform with intense particle fusion, suggesting the most effective sintering among all samples. This may be due to the closed environment retaining more vapor or transient liquid phases, thereby promoting maximum densification.

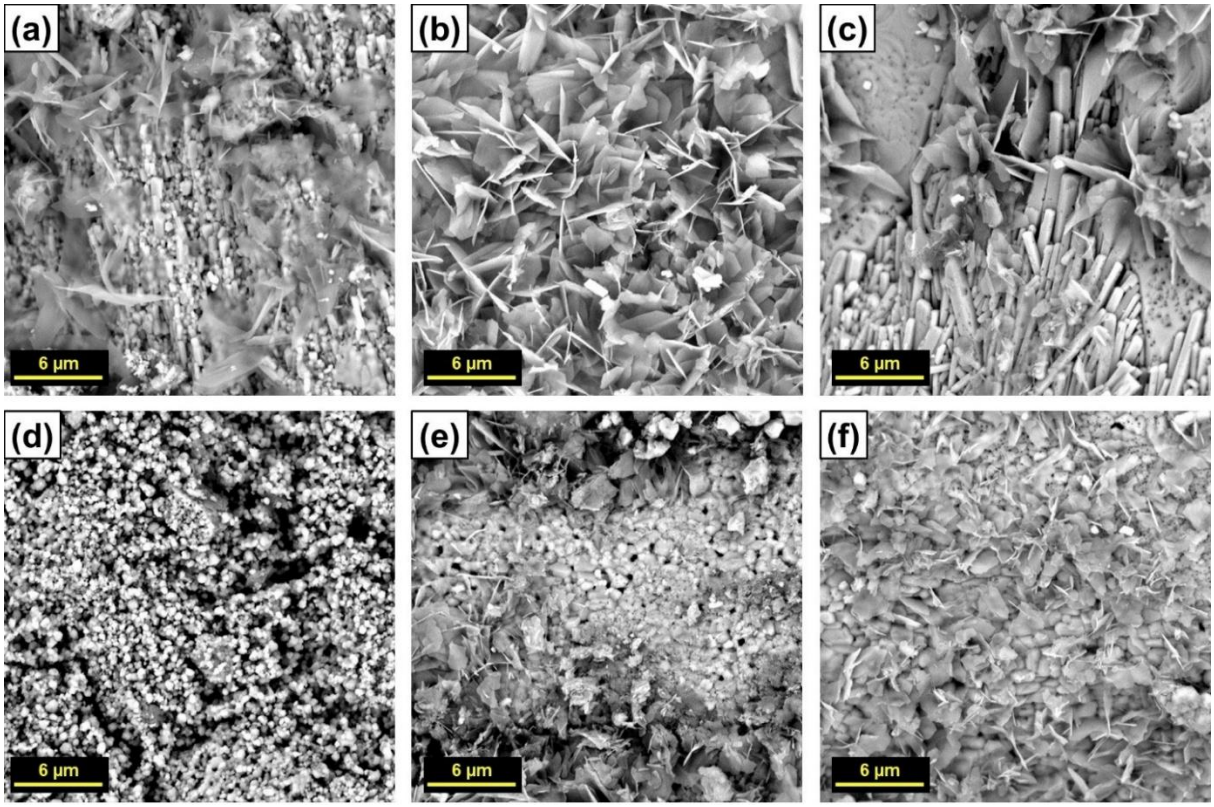

Figure 7. SEM image samples of the surfaces of (a) FBO-800, (b) FBO-900, (c) FBO-1000, (d) FBC-800, (e) FBC-900, and (f) FBC-1000.

In summary, increasing the sintering temperature from 800 °C to 1000 °C under both open and closed crucible conditions led to: (i) increased particle agglomeration, with particles forming larger clusters; (ii) morphological evolution from irregular or granular structures to more compact and oriented plate- or rod-like structures; and (iii) decreased surface porosity due to particle fusion and agglomeration. The key differences between FBO and FBC samples at the same temperature were mainly in the degree of agglomeration/densification and the types of structures formed. Closed sintering conditions (FBC) generally promoted more effective agglomeration and densification, resulting in denser and less porous materials compared to open sintering (FBO).

4. Conclusion

This study successfully synthesized hydroxyapatite (HA) from the bones of belida fish (*Chitala lopis*), a species abundant in Indonesian waters and commonly found as waste from local amplang production in Samarinda. Using a sintering method under two different atmospheres—open crucible (FBO) and closed crucible (FBC)—at temperatures ranging from 600°C to 1000°C, the influence of sintering conditions on the structural, morphological, and physicochemical properties of HA was thoroughly investigated. The results demonstrated that increasing sintering temperature improved the crystallinity and grain growth of HA, confirmed by XRD and FTIR analyses, with optimal crystallinity observed around 900°C for open sintering (FBO) and 800°C for closed sintering (FBC). SEM imaging revealed a clear evolution in morphology, with higher temperatures promoting particle agglomeration and densification,

DOI: https://doi.org/10.17509/ajse.v5i3.88775
p- ISSN 2776-6098 e- ISSN 2776-5938

while open sintering facilitated oriented crystal growth and larger crystallites. In contrast, closed sintering enhanced densification and reduced porosity, producing denser HA structures.

Trace elements such as Al, Fe, Zn, Ti, and K were detected in minor quantities, highlighting the natural complexity of HA derived from *Chitala lopis* bone and suggesting potential impacts on its bioactivity. These findings not only provide insight into optimizing sintering parameters for fish bone-derived HA but also contribute novel data on hydroxyapatite synthesized specifically from *Chitala lopis* bones, an underexplored natural resource. This work supports the sustainable valorization of fishery waste into high-value biomaterials with potential applications in biomedicine and environmental remediation.

5. ACKNOWLEDMENT

The authors gratefully acknowledge research funding provided by the Government of Indonesia through the Ministry of Research, Technology, and Higher Education [074/E5/PG.02.00.PL/2024] and DRPM Universitas Padjadjaran [3837/UN6.3.1/PT.00/2024]. This research was conducted as part of the requirements for the first author's graduation. During the study, the first author also received financial support from the Indonesian Education Scholarship (Beasiswa Pendidikan Indonesia), administered by the Ministry of Education, Culture, Research, and Technology (Kemendikbudristek) through the Higher Education Financing Center (Pusat Layanan Pembiayaan Pendidikan/PUSLAPDIK) and the Indonesia Endowment Fund for Education (Lembaga Pengelola Dana Pendidikan/LPDP).

6. AUTHORS' NOTE

The authors declare that there is no conflict of interest regarding the publication of this article. Authors confirmed that the paper was free of plagiarism.

7. REFERENCES

[1] Noviyanti, A. R., Akbar, N., Deawati, Y., Ernawati, E. E., Malik, Y. T., and Fauzia, R. P. (2020). A novel hydrothermal synthesis of nanohydroxyapatite from eggshell-calcium-oxide precursors. *Heliyon*, *6*(4), e03655.

[2] Sharifianjazi, F., Esmaeilkhanian, A., Moradi, M., Pakseresht, A., Asl, M. S., Karimi-Maleh, H., and Varma, R. S. (2021). Biocompatibility and mechanical properties of pigeon bone waste extracted natural nano-hydroxyapatite for bone tissue engineering. *Materials Science and Engineering: B*, *264*, 114950.

[3] Onuma, K., Makino, M., Sakamaki, I., Nakamura, M., Nishida, E., Tanaka, S., and Oyane, A. (2024). Ultrafast coating of fluoride-substituted hydroxyapatite layers on teeth by laser-assisted crystallization: Comparison of surface structure and composition among enamel, dentin, and cementum. *Applied Surface Science*, *674*, 160876.

[4] Wu, Y., and Bose, S. (2005). Nanocrystalline hydroxyapatite: micelle templated synthesis and characterization. *Langmuir*, *21*(8), 3232-3234.

[5] Dewi, A. H., and Ana, I. D. (2018). The use of hydroxyapatite bone substitute grafting for alveolar ridge preservation, sinus augmentation, and periodontal bone defect: A systematic review. *Heliyon*, *4*(10), e00884.

DOI: https://doi.org/10.17509/ajse.v5i3.88775
p- ISSN 2775-6793 e- ISSN 2775-6815

[6] Rodríguez-Lugo, V., Salinas-Rodríguez, E., Vázquez, R. A., Alemán, K., and Rivera, A. L. (2017). Hydroxyapatite synthesis from a starfish and β-tricalcium phosphate using a hydrothermal method. *RSC advances*, *7*(13), 7631-7639.

[7] Sadat-Shojai, M., Khorasani, M. T., Dinpanah-Khoshdargi, E., and Jamshidi, A. (2013). Synthesis methods for nanosized hydroxyapatite with diverse structures. *Acta biomaterialia*, *9*(8), 7591-7621.

[8] Fihri, A., Len, C., Varma, R. S., and Solhy, A. (2017). Hydroxyapatite: A review of syntheses, structure and applications in heterogeneous catalysis. *Coordination Chemistry Reviews*, *347*, 48-76.

[9] Kaneda, K., and Mizugaki, T. (2009). Development of concerto metal catalysts using apatite compounds for green organic syntheses. *Energy & Environmental Science*, *2*(6), 655-673.

[10] Watanabe, Y., Ikoma, T., Suetsugu, Y., Yamada, H., Tamura, K., Komatsu, Y., and Moriyoshi, Y. (2006). The densification of zeolite/apatite composites using a pulse electric current sintering method: A long-term assurance material for the disposal of radioactive waste. *Journal of the European Ceramic Society*, *26*(4-5), 481-486.

[11] Wu, H., Yan, H., Quan, Y., Zhao, H., Jiang, N., and Yin, C. (2018). Recent progress and perspectives in biotrickling filters for VOCs and odorous gases treatment. *Journal of Environmental Management*, *222*, 409-419.

[12] Shaaban, M., Van Zwieten, L., Bashir, S., Younas, A., Núñez-Delgado, A., Chhajro, M. A., and Hu, R. (2018). A concise review of biochar application to agricultural soils to improve soil conditions and fight pollution. *Journal of Environmental Management*, *228*, 429-440.

[13] Włóka, D., Placek, A., Smol, M., Rorat, A., Hutchison, D., and Kacprzak, M. (2019). The efficiency and economic aspects of phytoremediation technology using Phalaris arundinacea L. and Brassica napus L. combined with compost and nano SiO2 fertilization for the removal of PAH's from soil. *Journal of Environmental Management*, *234*, 311-319.

[14] Holkar, C. R., Jadhav, A. J., Pinjari, D. V., Mahamuni, N. M., and Pandit, A. B. (2016). A critical review on textile wastewater treatments: possible approaches. *Journal of Environmental Management*, *182*, 351-366.

[15] Kumari, M., Verma, R. K., and Roy, P. K. (2018). Effect of Carbafuran Pesticide on Mitotic Chromosomes of Mus musculus. *International Journal of Applied Sciences and Biotechnology*, *6*(2), 169-173.

[16] Venkatesan, J., Rekha, P. D., Anil, S., Bhatnagar, I., Sudha, P. N., Dechsakulwatana, C., and Shim, M. S. (2018). Hydroxyapatite from cuttlefish bone: isolation, characterizations, and applications. *Biotechnology and Bioprocess Engineering*, *23*(4), 383-393.

[17] Amenaghawon, A. N., Anyalewechi, C. L., Darmokoesoemo, H., and Kusuma, H. S. (2022). Hydroxyapatite-based adsorbents: Applications in sequestering heavy metals and dyes. *Journal of Environmental Management*, *302*, 113989.

[18] Ho, J. Y., Chang, T. T., Ho, P. C., Chang, H. K., and Chen, P. Y. (2024). Fabrication of gyroid-structured, hierarchically-porous hydroxyapatite scaffolds by a dual-templating method. *Materials Chemistry and Physics*, *314*, 128854.

DOI: https://doi.org/10.17509/ajse.v5i3.88775
p- ISSN 2776-6098 e- ISSN 2776-5938

[19] Wan, L., Cui, B., and Wang, L. (2024). A review on preparation raw materials, synthesis methods, and modifications of hydroxyapatite as well as their environmental applications. *Sustainable Chemistry and Pharmacy*, *38*, 101447.

[20] Huyen, D. T., Tien, D. X., and Thoai, D. Q. (2023). Bone-char from various food-waste: Synthesis, characterization, and removal of fluoride in groundwater. *Environmental Technology & Innovation*, *32*, 103342.

[21] Rashed, M. N., Gad, A. A. E., and Fathy, N. M. (2024). Efficiency of chemically activated raw and calcined waste fish bone for adsorption of Cd (II) and Pb (II) from polluted water. *Biomass Conversion and Biorefinery*, *14*(24), 31703-31720.

[22] Castillo-Paz, A. M., Gomez-Resendiz, M., Canon-Davila, D. F., Correa-Pina, B. A., Ramirez-Bon, R., and Rodriguez-Garcia, M. E. (2023). The effect of temperature on the physical-chemical properties of bovine hydroxyapatite biomimetic scaffolds for bone tissue engineering. *Ceramics International*, *49*(21), 33735-33747.

[23] Wagner, J., Luck, S., Loger, K., Açil, Y., Spille, J. H., Kurz, S., and Naujokat, H. (2024). Bone regeneration in critical-size defects of the mandible using biomechanically adapted CAD/CAM hybrid scaffolds: An in vivo study in miniature pigs. *Journal of Cranio-Maxillofacial Surgery*, *52*(1), 127-135.

[24] Alsaiari, R. A., Musa, E. M., and Rizk, M. A. (2023). Biodiesel production from date seed oil using hydroxyapatite-derived catalyst from waste camel bone. *Heliyon*, *9*(5), e15606.

[25] Pei, X., Wang, L., Wu, L., Lei, H., Zeng, Z., Wang, L., and Fan, Y. (2023). In-situ synthesized hydroxyapatite whiskers on 3D printed titanium cages enhanced osteointegration in a goat spinal fusion model. *Materials & Design*, *233*, 112270.

[26] Liaqat, S., Ahmed, Z., Umer, M. U., Ali, Q., Mustafa, M. F., Ferheen, I., and Waseem, M. (2024). Sheep bone valorization: Enhancing gastronomic sustainability through hydroxyapatite-enriched potato wedges. *International Journal of Gastronomy and Food Science*, *35*, 100841.

[27] Nurhadi, M., Kusumawardani, R., Wirhanuddin, W., Gunawan, R., and Nur, H. (2019). Carbon-containing hydroxyapatite obtained from fish bone as low-cost mesoporous material for methylene blue adsorption. *Bulletin of Chemical Reaction Engineering & Catalysis*, *14*(3), 660-671.

[28] Swamiappan, S., Xie, X., Lu, C., & Peng, X. (2025). Ultrasonic-assisted green synthesis and characterization of nano-hydroxyapatite from Cirrhinus molitorella fish scales bio-waste for biomedical applications. *Ceramics International*, *51*, 20452-20464.

[29] Sampath, V., and Krishnasamy, V. (2024). Synthesis and characterization of hydroxyapatite self-assembled nanocomposites on graphene oxide sheets from seashell waste: A green process for regenerative medicine. *Journal of the Mechanical Behavior of Biomedical Materials*, *151*, 106383.

[30] Wibisono, Y., Ummah, S. R., Hermanto, M. B., Djoyowasito, G., and Noviyanto, A. (2024). Slow-release hydroxyapatite fertilizer from crab shells waste for sustainable crop production. *Results in Engineering*, *21*, 101781.

[31] Esoso, A. A., Jen, T. C., Ikumapayi, O. M., Oladapo, B. I., and Akinlabi, E. T. (2023). Experimental analysis of nanostructured PEEK, African giant snail shell, and sea snail shell powder for hydroxyapatite formation for bone implant applications. *Composites Part C: Open Access*, *12*, 100398.

DOI: https://doi.org/10.17509/ajse.v5i3.88775
p- ISSN 2775-6793 e- ISSN 2775-6815

[32] Pon-On, W., Suntornsaratoon, P., Charoenphandhu, N., Thongbunchoo, J., Krishnamra, N., and Tang, I. M. (2016). Hydroxyapatite from fish scale for potential use as bone scaffold or regenerative material. *Materials Science and Engineering: C*, *62*, 183-189.

[33] Predoi, S. A., Ciobanu, S. C., Chifiriuc, M. C., Motelica-Heino, M., Predoi, D., and Iconaru, S. L. (2022). Hydroxyapatite nanopowders for effective removal of strontium ions from aqueous solutions. *Materials*, *16*(1), 229.

[34] Kamal, M. M., Mahmud, S., Plabon, I. A., Kader, M. A., and Islam, M. N. (2024). Effects of sintering temperature on the physical, structural, mechanical and antimicrobial properties of extracted hydroxyapatite ceramics from Anabas testudineus bone and head scull for biomedical applications. *Results in Materials*, *22*, 100590.

[35] Hussin, M. S. F., Idris, M. I., Abdullah, H. Z., Azeem, W., and Ghazali, I. (2023). Characterization and in vitro evaluation of hydroxyapatite from Fringescale sardinella bones for biomedical applications. *Journal of Saudi Chemical Society*, *27*(5), 101721.

[36] Trung, T. S., Minh, N. C., Cuong, H. N., Phuong, P. T. D., Dat, P. A., Nam, P. V., and Van Hoa, N. (2022). Valorization of fish and shrimp wastes to nano-hydroxyapatite/chitosan biocomposite for wastewater treatment. *Journal of Science: Advanced Materials and Devices*, *7*(4), 100485.

[37] Irwansyah, F. S., Noviyanti, A. R., Eddy, D. R., & Risdiana, R. (2022). Green template-mediated synthesis of biowaste nano-hydroxyapatite: a systematic literature review. *Molecules*, *27*(17), 5586.

[38] Errich, A., Azzaoui, K., Mejdoubi, E., Hammouti, B., Abidi, N., Akartasse, N., Benidire, L., EL Hajjaji, S., Sabbahi, R., and Lamhamdi, A. (2021). Toxic heavy metals removal using a hydroxyapatite and hydroxyethyl cellulose modified with a new Gum Arabic. *Indonesian Journal of Science and Technology*, *6*(1), 41-64.

[39] Irwansyah, F.S., Amal, A.I., Hadisantoso, E.P., Noviyanti, A.R., Eddy, D.R., Risdiana, R., Suryana, S., and Md Zain, S.B. (2023). How to make and characterize hydroxyapatite from eggshell using the hydrothermal method: potential insights for drug delivery system. *Indonesian Journal of Science and Technology*, *8*(3), 469-486.

[40] Waardhani, A.W., Noviyanti, A.R., Kusrini, E., Nugrahaningtyas, K.D., Prasetyo, A.B., Usman, A., Irwansyah, F.S., and Juliandri, J. (2025). A study on sustainable eggshell-derived hydroxyapatite/CMC membranes: Enhancing flexibility and thermal stability for sustainable development goals (SDGs*). Indonesian Journal of Science and Technology*, *10*(2), 191-206.

[41] Noviyanti, A.R., Adzkia, Q.A.A., Novella, I., Kurnia, I., Suryana, S., Ma'Amor, A.B., and Irwansyah, F.S. (2024). Hydroxyapatite as delivery and carrier material: Systematic literature review with bibliometric analysis. *ASEAN Journal of Science and Engineering*, *4*(2), 191-206.

[42] Le Ho, K. H., Dao, V. H., Pham, X. K., Nguyen, P. A., Phan, B. V., Doan, T. T., and Lam, T. H. (2022). Physicochemical properties, acute and subchronic toxicity of nano-hydroxyapatite obtained from Lates calcarifer fish bone. *Regional Studies in Marine Science*, *55*, 102560.

[43] Mathirat, A., Dalavi, P. A., Prabhu, A., GV, Y. D., Anil, S., Senthilkumar, K., and Venkatesan, J. (2022). Remineralizing potential of natural nano-hydroxyapatite obtained from epinephelus chlorostigma in artificially induced early enamel lesion: An in vitro study. *Nanomaterials*, *12*(22), 3993.

DOI: https://doi.org/10.17509/ajse.v5i3.88775
p- ISSN 2776-6098 e- ISSN 2776-5938

[44] Ahmed, F., Ali, I., Kousar, S., and Ahmed, S. (2022). The environmental impact of industrialization and foreign direct investment: empirical evidence from Asia-Pacific region. *Environmental Science and Pollution Research*, *29*(20), 29778-29792.

[45] Kazior, J. (2023). Influence of sintering atmosphere, temperature and the solution-annealing treatment on the properties of precipitation-hardening sintered 17-4 PH stainless steel. *Materials*, *16*(2), 760.

[46] Yusuf, A., Muhammad, N. M., Noviyanti, A. R., and Risdiana, R. (2020). The effect of temperature synthesis on the purity and crystallinity of hydroxyapatite. *Key Engineering Materials*, *860*, 228-233.

[47] Chen, H., Wang, R., Qian, L., Liu, H., Wang, J., and Zhu, M. (2020). Surface modification of urchin-like serried hydroxyapatite with sol-gel method and its application in dental composites. *Composites Part B: Engineering*, *182*, 107621.

[48] Idris, N., Dan-Asabe, B., Osseni, S. A., Rabiu, K. O., Sowunmi, A. R., Bansod, N. D., and Obada, D. O. (2025). Properties of natural hydroxyapatite prepared by pressureless sintering using different temperatures and holding times. *Next Nanotechnology*, *7*, 100168.

[49] Bas, M., Daglilar, S., Kuskonmaz, N., Kalkandelen, C., Erdemir, G., Kuruca, S. E., and Ficai, A. (2020). Mechanical and biocompatibility properties of calcium phosphate bioceramics derived from salmon fish bone wastes. *International Journal of Molecular Sciences*, *21*(21), 8082.

[50] Boutinguiza, M., Pou, J., Comesaña, R., Lusquiños, F., De Carlos, A., and León, B. (2012). Biological hydroxyapatite obtained from fish bones. *Materials Science and Engineering: C*, *32*(3), 478-486.

[51] Kusumawardani, R., Noviyanti, A. R., Nurhadi, M., and Umar, A. A. (2023). Effect of Preparation Acetone on Fish Bones Synthesized Through Sintering Method to Improve Hydroxyapatite Characteristics. *al Kimiya: Jurnal Ilmu Kimia dan Terapan*, *10*(2), 87-97.

[52] Sathiyavimal, S., Vasantharaj, S., Shanmugavel, M., Manikandan, E., Nguyen-Tri, P., Brindhadevi, K., and Pugazhendhi, A. (2020). Facile synthesis and characterization of hydroxyapatite from fish bones: Photocatalytic degradation of industrial dyes (crystal violet and Congo red). *Progress in Organic Coatings*, *148*, 105890.

[53] Fatimah, S., Ragadhita, R., Al Husaeni, D. F., and Nandiyanto, A. B. D. (2022). How to calculate crystallite size from x-ray diffraction (XRD) using Scherrer method. *ASEAN Journal of Science and Engineering*, *2*(1), 65-76.

[54] Fernández-Arias, M., Álvarez-Olcina, I., Malvido-Fresnillo, P., Vázquez, J. A., Boutinguiza, M., Comesaña, R., and Pou, J. (2021). Biogenic calcium phosphate from fish discards and by-products. *Applied Sciences*, *11*(8), 3387.

[55] Hammood, A. S., Hassan, S. S., Alkhafagy, M. T., and Jaber, H. L. (2019). Effect of calcination temperature on characterization of natural hydroxyapatite prepared from carp fish bones. *SN Applied Sciences*, *1*(5), 1-12.

[56] Ooi, C. Y., Hamdi, M., and Ramesh, S. (2007). Properties of hydroxyapatite produced by annealing of bovine bone. *Ceramics international*, *33*(7), 1171-1177.

[57] Abdin, Y., Usman, A., Ok, Y. S., Tsang, Y. F., and Al-Wabel, M. (2020). Competitive sorption and availability of coexisting heavy metals in mining-contaminated soil: Contrasting effects of mesquite and fishbone biochars. *Environmental Research*, *181*, 108846.

DOI: https://doi.org/10.17509/ajse.v5i3.88775
p- ISSN 2775-6793 e- ISSN 2775-6815

[58] Khamkongkaeo, A., Boonchuduang, T., Klysubun, W., Amonpattaratkit, P., Chunate, H. T., Tuchinda, N., and Lohwongwatana, B. (2021). Sintering behavior and mechanical properties of hydroxyapatite ceramics prepared from Nile Tilapia (Oreochromis niloticus) bone and commercial powder for biomedical applications. *Ceramics International*, *47*(24), 34575-34584.

[59] Wang, Z., Wang, Y., Ito, Y., Zhang, P., and Chen, X. (2016). A comparative study on the in vivo degradation of poly (L-lactide) based composite implants for bone fracture fixation. *Scientific reports*, *6*(1), 20770.

[60] Chaair, H., Labjar, H., and Britel, O. (2017). Synthesis of β-tricalcium phosphate. *Morphologie*, *101*(334), 120-124.

[61] Jalota, S., Tas, A. C., and Bhaduri, S. B. (2005). Synthesis of HA-Seeded TTCP (Ca4(PO4) 2O) Powders at 1230° C from Ca (CH3COO) 2· H2O and NH4H2PO4. *Journal of the American Ceramic Society*, *88*(12), 3353-3360.

[62] Ara, K. A., Takahiro, T., Diki, P. M., Norio, S., and Nobuhiro, K. (2023). Synthesis and characterization of columbite type solid solution structured niobate Mg 1− x Ca x Nb 2 O 6. *Journal of the Ceramic Society of Japan*, *131*(8), 355-362.

[63] Mulus, D. A. S., Permana, M. D., Hayaa'Prawiranegara, S. P., Tustika, C. Z., Putri, S. P., Zahra, S. A., and Eddy, D. R. (2025). Enhanced performance of spin-coated silver-modified titanium dioxide thin films over dip coating method for metformin photodegradation. *Results in Optics*, 100838.

[64] Maesaroh, K., Permana, M. D., Eddy, D. R., and Rahayu, I. (2023). The effect of different synthesis with chemical and biological methods on properties of silver oxide nanoparticles. *Trends in Sciences*, *20*(3), 4350-4350.

[65] Boukhvalov, D. W., Paolucci, V., D'Olimpio, G., Cantalini, C., and Politano, A. (2021). Chemical reactions on surfaces for applications in catalysis, gas sensing, adsorption-assisted desalination and Li-ion batteries: opportunities and challenges for surface science. *Physical Chemistry Chemical Physics*, *23*(13), 7541-7552.

[66] Liu, X., Xia, Z., Wang, Y., Luo, D., Li, Z., Meng, Z., and Lian, H. (2024). Zinc-doped inorganic bioactive materials: a comprehensive review of properties and their applications in osteogenesis, antibacterial, and hemostasis. *Applied Materials Today*, *40*, 102393.

[67] Balakrishnan, S., Padmanabhan, V. P., Kulandaivelu, R., Nellaiappan, T. S. N., Sagadevan, S., Paiman, S., and Oh, W. C. (2021). Influence of iron doping towards the physicochemical and biological characteristics of hydroxyapatite. *Ceramics International*, *47*(4), 5061-5070.

[68] Mostafa, N. Y. (2005). Characterization, thermal stability and sintering of hydroxyapatite powders prepared by different routes. *Materials Chemistry and Physics*, *94*(2-3), 333-341.

[69] Ressler, A., Žužić, A., Ivanišević, I., Kamboj, N., & Ivanković, H. (2021). Ionic substituted hydroxyapatite for bone regeneration applications: A review. *Open Ceramics*, *6*, 100122.

[70] Cotrut, C. M., Blidisel, A., Vranceanu, D. M., Vladescu, A., Ungureanu, E., Pana, I., and Titorencu, I. (2024). Evaluation of the in vitro behavior of electrochemically deposited plate-like crystal hydroxyapatite coatings. *Biomimetics*, *9*(11), 704.

DOI: https://doi.org/10.17509/ajse.v5i3.88775
p- ISSN 2776-6098 e- ISSN 2776-5938